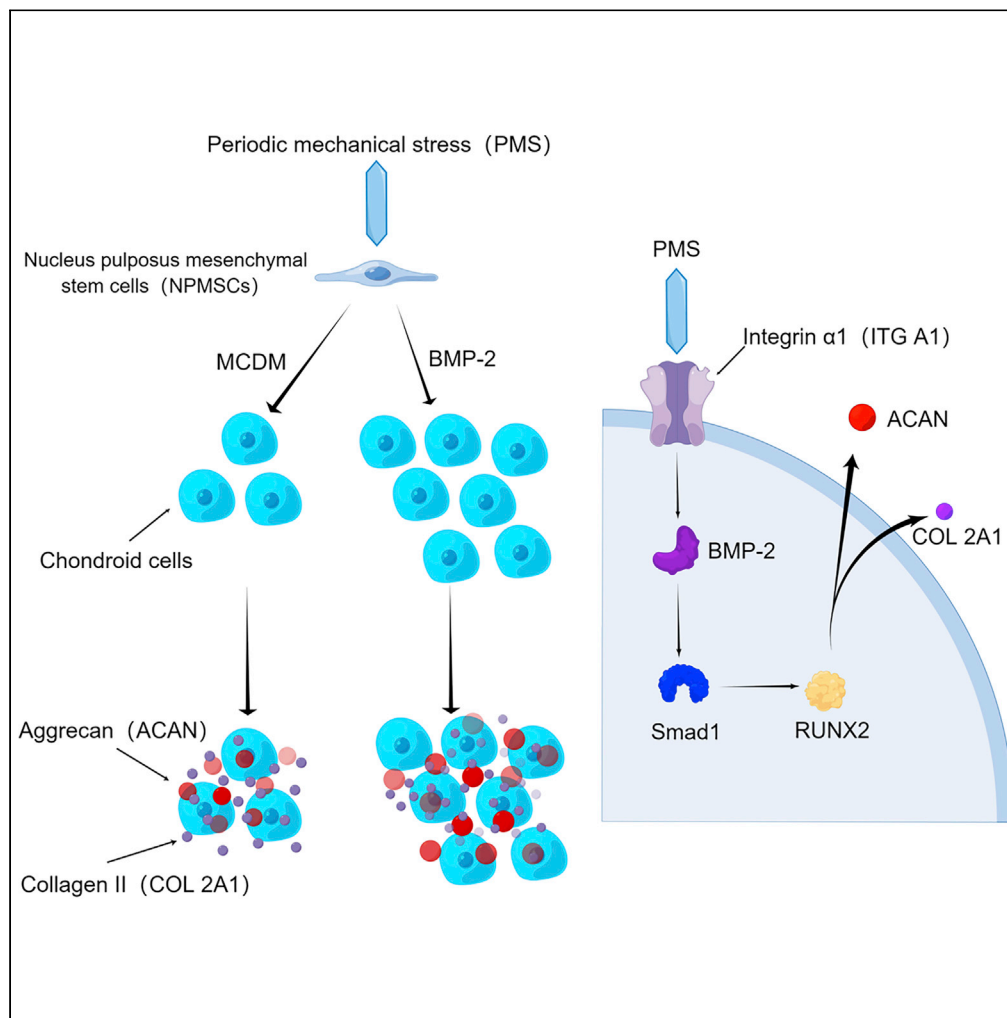CellPress
OPEN ACCESS

Article

Construction of tissue-engineered nucleus pulposus by stimulation with periodic mechanical stress and BMP-2

Yang Liu, Gong-ming Gao, Kai-yuan Yang, Lu-ming Nong

l1uyyang031995@gmail.com

Highlights
Extraction of NPMSCs from degenerated nucleus pulposus

NPMSCs cultured *in vitro* by simulating physiological mechanical stress

ITG A1 to promote proliferation and differentiation of NPMSCs through BMP-2/Smad1/ RUNX2

Injectable tissue-engineered nucleus pulposus

Article

Construction of tissue-engineered nucleus pulposus by stimulation with periodic mechanical stress and BMP-2

Yang Liu,[1,2,3] Gong-ming Gao,[1,3] Kai-yuan Yang,[1] and Lu-ming Nong[1,4,*]

SUMMARY

Intervertebral disc (IVD) degeneration, which is common among elderly individuals, mainly manifests as low back pain and is caused by structural deterioration of the nucleus pulposus (NP) due to physiological mechanical stress. NP mesenchymal stem cells (NPMSCs) around the IVD endplate have multidirectional differentiation potential and can be used for tissue repair. To define favorable conditions for NPMSC proliferation and differentiation into chondroid cells for NP repair, the present study simulated periodic mechanical stress (PMS) of the NP under physiological conditions using MSC chondrogenic differentiation medium and recombinant human BMP-2 (rhBMP-2). rhBMP-2 effectively promoted NPMSC proliferation and differentiation. To clarify the mechanism of action of rhBMP-2, integrin alpha 1 (ITG A1) and BMP-2 were inhibited. PMS regulated the BMP-2/Smad1/RUNX2 pathway through ITG A1 and promoted NPMSC proliferation and differentiation. During tissue-engineered NP construction, PMS can effectively reduce osteogenic differentiation and promote extracellular matrix protein synthesis to enhance structural NP recovery.

INTRODUCTION

Low back pain (LBP) is a common chronic condition experienced by more than 80% of adults at some point in their lifetime and is one of the main causes of activity limitation in patients below the age of 45 years (Kadow et al., 2015). Intervertebral disc degeneration (IVDD) is the primary cause of LBP, representing the pathological process leading to the deterioration of intervertebral connective tissue, which plays an essential role in kinematics of the spine (Cazzanelli and Wuertz-Kozak, 2020). Degeneration occurs at the tissue, cellular, and molecular levels, resulting in substantial modifications to the physiology and morphology of the intervertebral disc (IVD), ultimately reducing the ability of the IVD to withstand loading. IVDD is a multifactorial disease, and the etiology and pathogenesis of IVDD are incompletely understood. However, scientists generally consider that genetic factors, age, lifestyle, and non-physiological mechanical loading are the main factors of IVDD (Clouet et al., 2009; Sekine et al., 2021; Hadjipavlou et al., 2008). It is estimated that $50 billion in direct costs will be incurred globally each year for the treatment of this disease (Dieleman et al., 2016); taking into account indirect costs of reduced patient productivity caused by disability, the economic impact of LBP is a substantial challenge around the world (Katz, 2006).

Currently, discectomy is the standard intervention for IVDD, and this approach can relieve the clinical symptoms but does not address the underlying disease. Similarly, the use of sutures or rigid implants to prevent early re-herniation after discectomy has been shown to be effective; however, these devices cannot promote tissue healing and therefore cannot prevent degeneration, as demonstrated in long-term clinical trials (Ahlgren et al., 2000; Chiang et al., 2011; Parker et al., 2016). Hence, tissue-engineered nucleus pulposus (NP) has attracted the attention of a large number of researchers to prevent re-herniation after discectomy and promote the healing and remodeling of degenerative discs (Ledet et al., 2009; Oehme et al., 2014; Hegewald et al., 2015). Hydration of the NP is crucial to repair the mechanical function of these discs, and a variety of injectable biomaterials and stem cell-based therapies have been developed to restore hydration of the NP in IVDD (Ahrens et al., 2009; Su et al., 2010; Zhou et al., 2018; Feng et al., 2012). Cells and scaffolds alone are insufficient; hence, growth factors, which stimulate cells to perform appropriate tasks, are another important component of tissue engineering strategies.

[1]Department of Orthopedics, The Affiliated Changzhou No.2 People's Hospital of Nanjing Medical University, No.29 Xinglong Lane, Tianning District, Changzhou, Jiangsu Province 213000, P.R. China

[2]Dalian Medical University, No. 9 West Section of South Lvshun Road, Lvshunkou District, Dalian, Liaoning Province 116044, P.R. China

[3]These authors contributed equally

[4]Lead contact

*Correspondence:
l1uyyang031995@gmail.com

https://doi.org/10.1016/j.isci.2022.104405

Bone morphogenetic proteins (BMPs) are osteogenic inducers frequently used in the clinic. To date, a variety of BMPs and BMP antagonists have been shown to work together to promote bone regeneration (Wu et al., 2016; Brazil et al., 2015; Worthley et al., 2015). Recombinant human BMP-2 (rhBMP-2) was approved by the US Food and Drug Administration (FDA) as early as 2002 to promote bone fusion in anterior lumbar interbody fusion (Cheng et al., 2003). However, the application of BMP-2 itself at a physiological dose is insufficient, and higher doses may cause many adverse events, such as excessive growth, abnormal osteogenesis, abnormal osteoclast activation, vertebral osteolysis, and local bone and wound inflammation and edema (Poynton and Lane, 2002; Govender et al., 2002). Nevertheless, there have been no reports of systemic effects caused by topical application of BMP-2. The half-life of BMP-2 administered in buffer alone to non-primates is only 7 min (Lo et al., 2012). The results of *in vitro* experiments with human NP cells (NPCs) have shown that BMP-2 can promote the formation of osteoblasts from a monolayer of NPCs; however, when the number of cells increases, inhibitors in the cells or extracellular matrix (ECM) may inhibit bone formation (Brown et al., 2020).

Our previous study demonstrated that periodic mechanical stress (PMS) can promote the proliferation and ECM secretion of NPCs cultured *in vitro*. Therefore, we designed and tested a compression device for use in cell culture *in vitro*. This external compression device was used in the present study to simulate the mechanical stress placed on NPs with normal activity by measuring the expression of BMP-2 and ECM-related proteins and to investigate the optimal concentration of exogenous BMP-2 as a cytokine in tissue engineering. We also designed relevant experiments to demonstrate that NP mesenchymal stem cells (NPMSCs) activate the BMP-2/Smad1/RUNX2 pathway by upregulating integrin alpha 1 (ITG A1) expression to stimulate proliferation, differentiation, and ECM synthesis under PMS. The present study provides new information about stress-related signaling in NPMSCs and the use of injectable tissue-engineered NP for the treatment of IVDD.

RESULTS

Identify stemness markers and proliferation competence in NPMSCs

To determine whether the obtained cells were NPMSCs, we characterized the first generation of cells according to the standards established by the ISCT. First, the cells exhibited plastic-adherent growth. Second, we used flow cytometry to identify the cell surface antigens, including CD105, CD73, and CD90 expression and no CD45, CD34, or HLA-DR surface molecule expression (Figures 1A and 1B). Under the conditions of normal cell culture, the CCK-8 assay results showed that the number of cells gradually increased and was significantly higher on day 5 than on days 3 and 1. The value-added rate (the ratio of the CCK-8 signals in each group) was used to assess growth. The value-added rate reached its peak on day 5 and was slightly decreased on day 7; however, the rate remained significantly higher than that on days 1 and 3 (Figure 1C). The decrease in proliferation on day 7 was due to the rapid growth of the cells and inhibition of growth by intercellular contact. We also assayed the mRNA expression of ECM-related genes, which gradually increased over time (Figure 1D). Furthermore, we tested the differentiation ability of NPMSCs using western blotting (Figure 1E). The results showed that the NPMSCs differentiated into NP cells and expressed collagen II and aggrecan proteins in MCDM (Figures 1F and 1G).

PMS enhances NPMSCs proliferation and promotes NPMSCs differentiation

To determine whether normal spinal physiological pressure promotes the proliferation and differentiation of NPMSCs, PMS in the normal spine was reconstructed using an experimental model. The cells were cultured in MCDM and under PMS conditions. The CCK-8 assay results showed that on days 5 and 7, the proliferation rate in the PMS group was significantly higher than that in the MCDM group (Figure 2A). At the same time, the expression levels of COL 2A1 and ACAN in the two groups were detected by RT-PCR. The results showed that the RNA expression levels were significantly higher in the PMS group than in the MCDM group (Figure 2B). Finally, we used western blotting to quantify the protein expression (Figure 2C). The results showed that the expression levels of collagen II and aggrecan in the PMS group were significantly higher than those in the MCDM group. In each test, the combined effect of the two conditions was better than that of either condition alone, and the differences were statistically significant (Figures 2D, 2E, and 2F).

NPMSCs promoted proliferation and differentiation by BMP-2

To determine whether BMP-2 promotes the proliferation and differentiation of NPMSCs and to estimate the optimal concentration of rhBMP-2, we used various concentrations of rhBMP-2 to culture NPMSCs and compared the results with those in the normal control (NC) and MCDM groups (Figure 3A). The
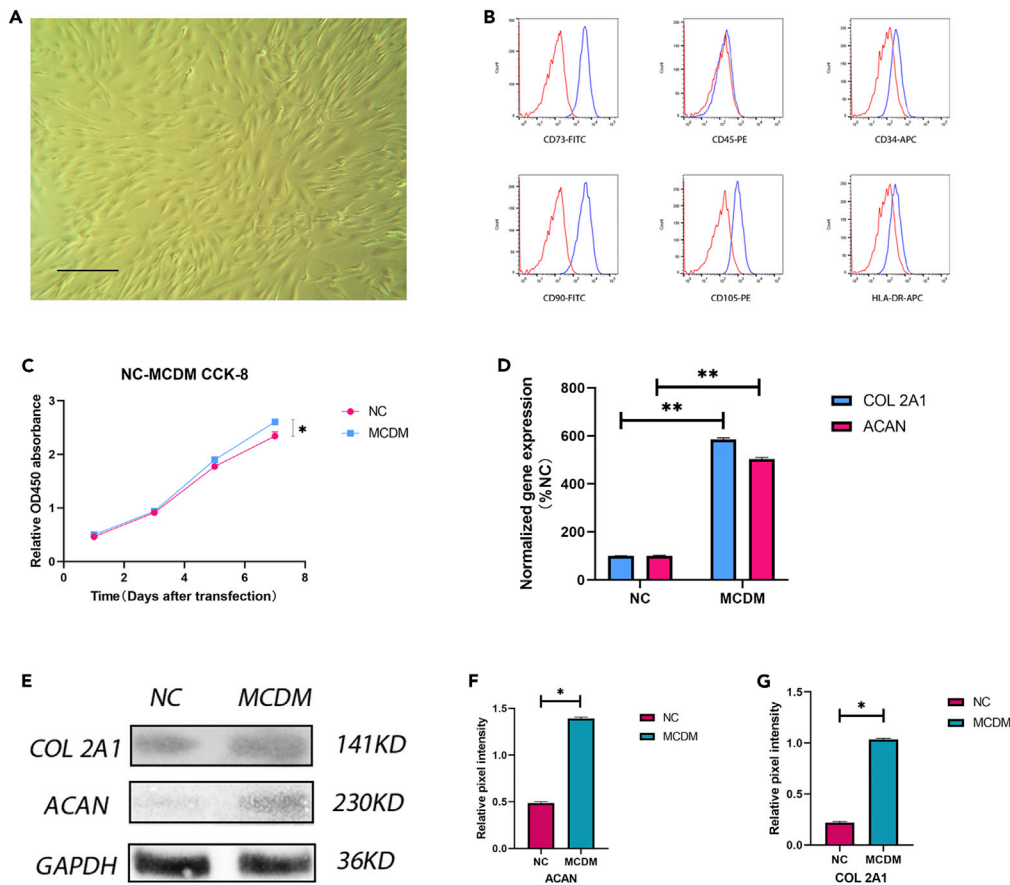
Figure 1. Stem cell identification and proliferation and differentiation tests

(A) Cell morphology under a light microscope. Magnification: 40×. Scale bar: 50 μm.

(B) Cell surface markers (CD90, CD105, CD73, CD34, CD45, and HLA-DR) of NPMSCs were detected by flow cytometry.

(C) The cell proliferation rate was measured by CCK-8 assay. The number of cells gradually increased and was significantly higher on day 5 than on days 3 and 1. The value-added rate (CCK-8 signal ratio) was used to assess the number of cells. The value-added rate reached a peak on day 5 and was slightly decreased on day 7; however, the rate remained significantly higher than that on days 1 and 3. Results are presented as the mean ± SD of three independent experiments (*p<0.05).

(D) Levels of COL 2A1 and ACAN mRNA expression under the normal and MCDM culture conditions were detected by quantitative RT–PCR. Under the MCDM conditions, the levels of COL 2A1 and ACAN mRNA expression were effectively increased. Results are presented as the mean ± SD of three independent experiments (**p<0.01).

(E–G) The protein levels of COL 2A1 and ACAN were analyzed by western blotting (E), and the relative quantitative data (F, G) were calculated. GAPDH was used as an internal control. Results are presented as the mean ± SD of three independent experiments (*p < 0.05).

comparison showed that the concentration of rhBMP-2 that had the best effect on the proliferation and differentiation of NPMSCs was 200 ng/mL, with significant differences compared with the MCDM and NC groups (Figures 3B and 3C). In addition, we knocked down BMP-2 in the cells and verified the knockdown after NPMSCs were exposed to PMS during differentiation (Figures 3D and 3E). The results showed that ECM synthesis by NPMSCs was significantly decreased after BMP-2 was knocked down; thus, the differentiation ability of the cells was decreased, and this result was statistically significant (Figures 3F, 3G, and 3H). Finally, we used immunofluorescence to label BMP-2 in the cells (Figure 3I); under PMS, the content of BMP-2 in the cells was significantly increased, and the fluorescence intensity was significantly higher than that in two other groups (Figure 3J). These differences were statistically significant.

Fibrinogen and thrombin to construct a tissue-engineered nucleus pulposus

To determine the concentration of fibrin gel that can promote cell adhesion and growth, we assessed the structure of the fibrin gel scaffolds at various concentrations by scanning electron microscopy and
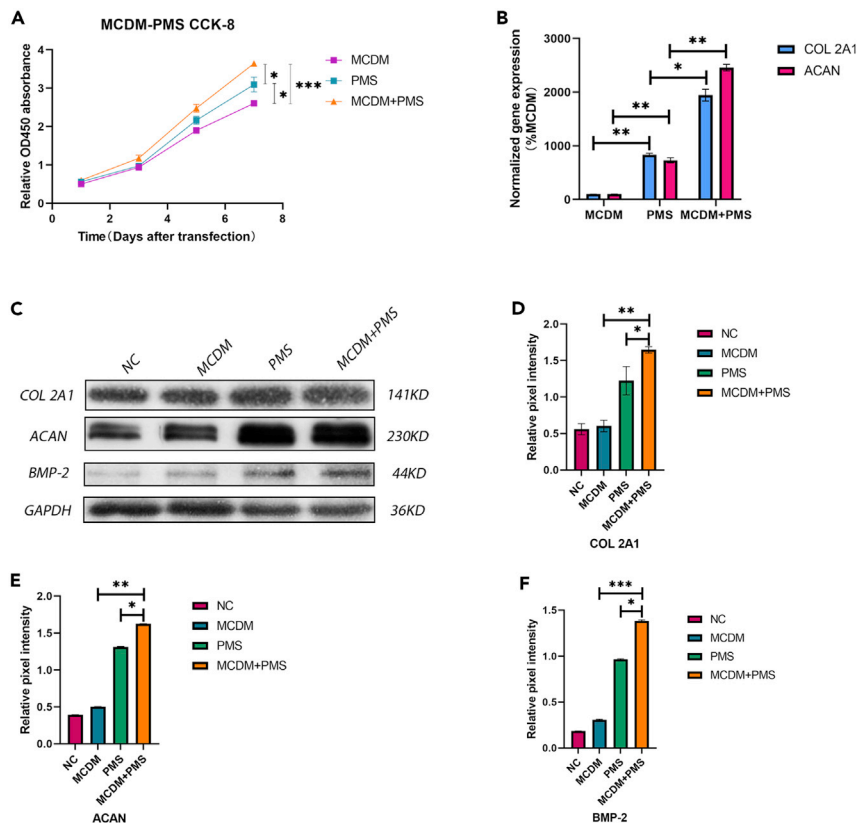
Figure 2. PMS effectively promoted the proliferation and differentiation of NPMSCs

(A) The CCK-8 assay results showed that the rate of proliferation was significantly higher in the PMS group than in the MCDM group on days 5 and 7, and the rate of proliferation was significantly increased when MCDM was combined with PMS. Results are presented as the mean $\pm$ SD of three independent experiments (*$p < 0.05$, ***$p < 0.001$).

(B) The levels of COL 2A1 and ACAN mRNA expression in the MCDM, PMS, and MCDM + PMS groups were detected by quantitative RT–PCR. The results showed that the mRNA expression of COL 2A1 and ACAN was significantly increased in the MCDM + PMS group compared with that in two other groups. Results are presented as the mean $\pm$ SD of three independent experiments (*$p < 0.05$, **$p < 0.01$). (A–B) MCDM was used as an internal control.

(C–F) The protein levels of COL 2A1, ACAN, and BMP-2 were analyzed by western blotting (C), and the relative quantitative data (D–F) were calculated. GAPDH was used as an internal control. Results are presented as the mean $\pm$ SD of three independent experiments (*$p < 0.05$, **$p < 0.01$, ***$p < 0.001$).

monitored cell adhesion and growth after inoculation (Figure 4A). The results showed that the fibrin gel scaffold with a final concentration of 50 mg/mL induced the highest levels of cell adhesion and growth (Figure 4B). Finally, to verify whether the proliferation and differentiation of NPMSCs could be promoted by the tissue-engineered NP under PMS, we performed immunohistochemistry and imaged the sections after the addition of BMP-2. Pure tissue-engineered NP was used as a control. The results showed significantly better proliferation and differentiation of NPMSCs in tissue-engineered NP treated with both BMP-2 and PMS than in the other two groups (Figure 4C).

Regulation of proliferation, differentiation, and ECM expression of NPMSC by PMS activation of ITGA1 via BMP-2/SMAD1/Runx2 axis

To explore the mechanism by which these conditions promoted NPMSC proliferation, differentiation, and ECM synthesis, we conducted a series of protein expression experiments. Initially, we detected the downstream proteins associated with BMP-2, including Smad1 and RNUX2, in the presence of PMS alone, BMP-2 alone, and a combination of BMP-2 and PMS (Figure 5A). Normal culture conditions were used as the control. The results showed that Smad1 and RUNX2 levels were significantly higher in the group with both BMP-2 and PMS than in the other three groups (Figure 5B). Then, we knocked down ITG A1 (Figures 5C, 5D, and 5E); the results showed that the expression of BMP-2 was decreased under PMS conditions after
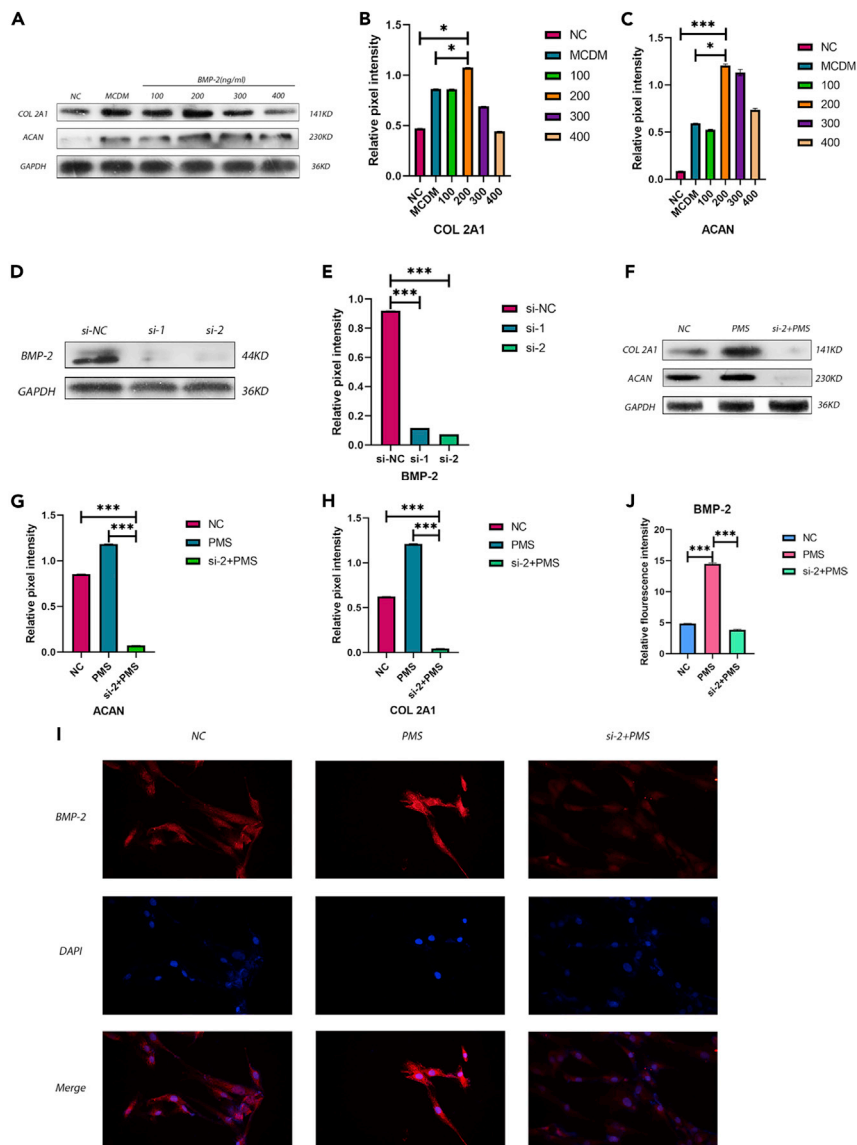
Figure 3. BMP-2 stimulated the proliferation and differentiation of NPMSCs

(A–C) The protein levels of COL 2A1 and ACAN were assayed by western blotting (A), and the relative quantitative data (B and C) were calculated. GAPDH was used as an internal control. The results showed that the protein expression of COL 2A1 and ACAN at 200 ng/mL rhBMP-2 was higher than that in the other groups. Results are presented as the mean ± SD of three independent experiments (*p < 0.05, ***p < 0.001).

(D and E) BMP-2 was knocked down using a silencing agent. The reagent effectively reduced the expression of BMP-2 protein in the cells. Results are presented as the mean ± SD of three independent experiments (***p < 0.001).

(F–H) The protein expression of COL 2A1 and ACAN was significantly decreased after BMP-2 knockdown under PMS. Results are presented as the mean ± SD of three independent experiments (***p < 0.001).

(I–J) Representative images of immunofluorescence staining for BMP-2 were obtained; and the relative fluorescence intensity in each group was calculated. Results are presented as the mean ± SD of three independent experiments (***p < 0.001).

ITG A1 knockdown and that the expression of the downstream proteins Smad1/RUNX2 and ECM proteins COL2A1 and ACAN was also decreased (Figure 5F). Finally, we knocked down BMP-2 again for verification (Figure 5G). The results showed that the expression of ITG A1 was not influenced by the knockdown of BMP-2; however, the expression of Smad1/RUNX2 and the ECM proteins COL2A1 and ACAN was
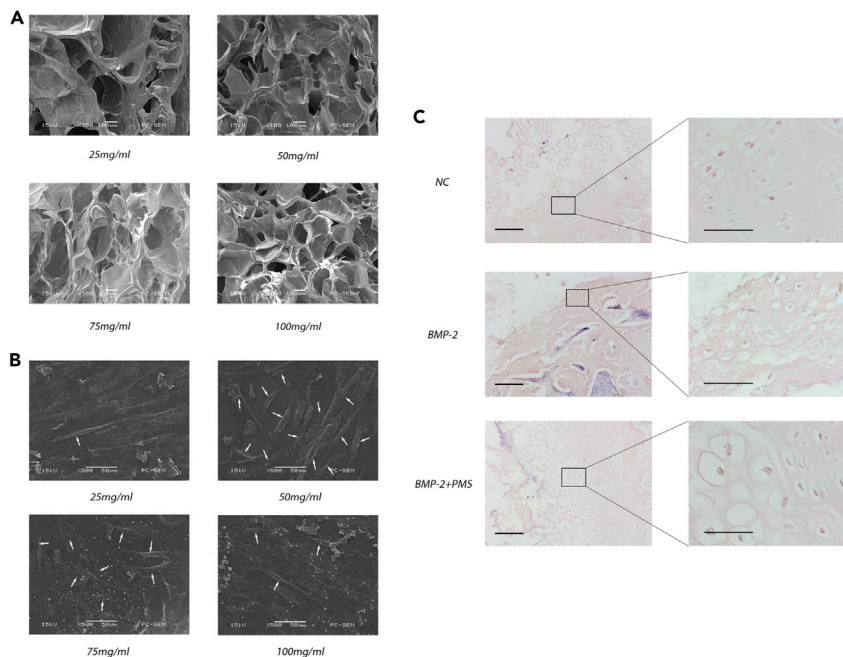
Figure 4. Construction of tissue-engineered NP by NPMSCs and the chitosan composite fibrin gel scaffold
(A) Representative images of the fibrin gel scaffolds at various concentrations were acquired by electron microscopy.
(B) Representative electron micrographs of tissue-engineered NP constructed by NPMSCs and the chitosan composite fibrin gel scaffold. The growth of NPMSCs was better than that in the other groups when the concentration of the chitosan composite fibrin gel scaffold was 50 mg/mL. The white arrows indicate cells attached to the scaffold.
(C) Representative histological images of tissue-engineered NP were obtained. Alone used BMP-2 can promote the differentiation of cartilage-like cells, also cause its osteogenic differentiation. Under the combined action of PMS, osteogenic differentiation was obviously inhibited. Magnification: 40✕ (left), 200 ✕ (right). Scale bars: 50 and 20 μm for low and high magnification, respectively. Determination of sustained release performance of scaffolds see also Figure S2.

decreased (Figure 5H). This finding indicated that PMS activation of ITG A1 regulated NPMSC proliferation, differentiation, and ECM synthesis via the BMP-2/SMAD1/RUNX2 axis.

DISCUSSION

Numerous studies have shown that the microenvironment of the IVD, including excessive mechanical stress, high osmolality, inflammation, and malnutrition, is responsible for a decrease in the number of NP cells and an increase in ECM (Mwale et al., 2011; Le Maitre et al., 2007; Wuertz et al., 2007). The levels of proteoglycan and collagen in the IVD matrix decrease rapidly during IVDD, leading to biomechanical changes in the IVD and a series of other alterations, such as an increase in osmotic pressure (Neidlinger-Wilke et al., 2012). Therefore, excessive mechanical stress plays an important role in the process of IVDD. Adipose-derived MSCs and bone marrow MSCs are potential sources of cells for the treatment of IVDD; however, the survival and function of these cells are severely limited by excessive mechanical stress (Leung et al., 2006; Hoogendoorn et al., 2008). Our previous studies demonstrated that the survival and function of NP cells were not affected by excessive mechanical stress; however, the proliferative ability of these cells was enhanced (Gao et al., 2016). In the present study, we used NP-derived stem cells as seed cells, which survived and functioned better under the conditions of stress than under the stress-free conditions. This phenomenon also indicates that NP-derived stem cells can be used as seed cells in tissue engineering.

MSCs are stromal cells with multidirectional differentiation potential that can differentiate into osteoblasts, chondrocytes, myocytes, and adipocytes (Caplan, 2017). Bone marrow and fat-derived MSCs can achieve IVD-like phenotypes after intradiscal transplantation by maintaining cellular activity and proliferation and can provide chondrocyte cues to promote regeneration. These processes have been successfully demonstrated in animal models (Cunha et al., 2017; Sakai et al., 2005; Zhang et al., 2011; Chen et al., 2016).
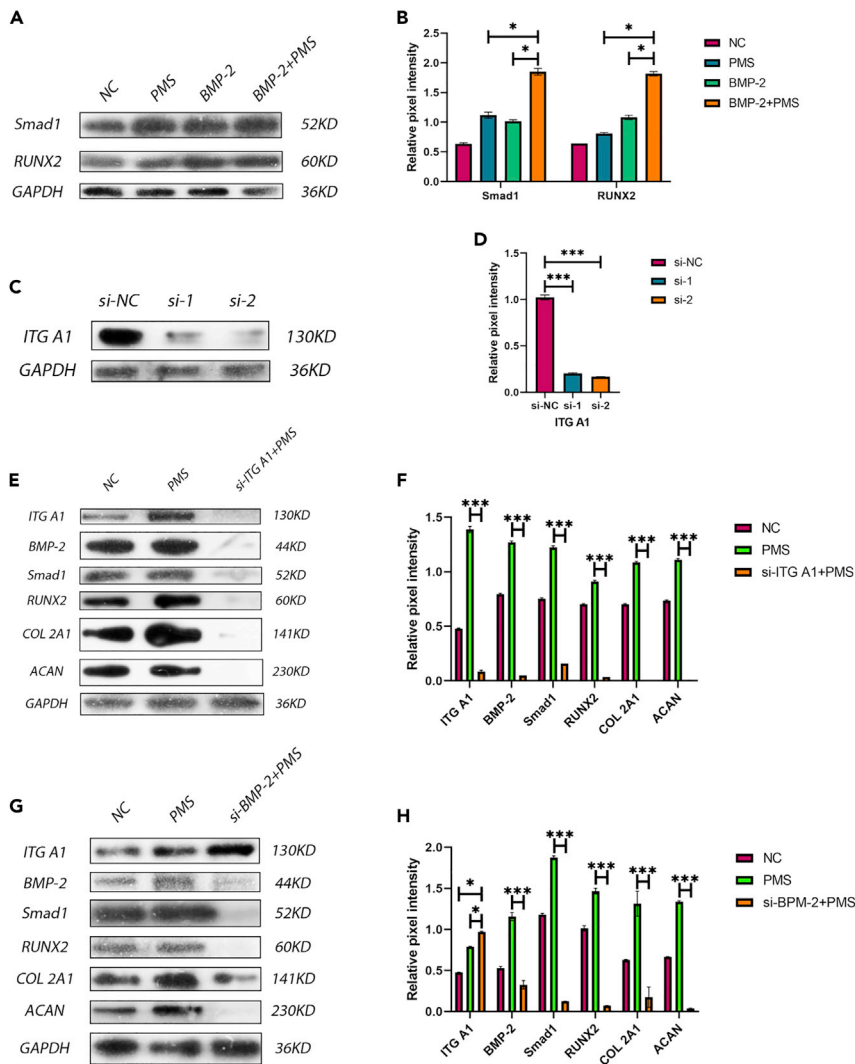
Figure 5. PMS promoted the proliferation and differentiation of NPMSCs through activation of the BMP-2/Smad1/Runx2 axis by ITG A1

(A–H) The protein levels of Smad1, RUNX2, ITG A1, BMP-2, COL 2A1, and ACAN were analyzed by western blotting (A, C, E, G), and the relative quantitative data (B, D, F, H) were calculated. GAPDH was used as an internal control. (A–B) BMP-2 + PMS effectively promoted the expression of SMAD1 and Runx2. Results are presented as the mean ± SD of three independent experiments (*p < 0.05). (C–D) The knockdown reagent effectively reduced the expression of ITG A1. Results are presented as the mean ± SD of three independent experiments (***p < 0.001). (E–F) The expression of all proteins was decreased when ITG A1 was knocked down. Results are presented as the mean ± SD of three independent experiments (***p < 0.001). (G–H) The protein expression of ITG A1 was not influenced by the knockdown of BMP-2, and the expression of other proteins was decreased. Results are presented as the mean ± SD of three independent experiments (*p < 0.05, ***p < 0.001).

However, the trend of hypertrophic differentiation of MSCs remains a common problem that affects the beneficial outcome of MSC-based healing (Murdoch et al., 2007). To solve this problem, Risbud et al. proposed the use of notochordal cells for transplantation therapy (Risbud and Shapiro, 2011), and Bach et al. proved that notochordal cells could regenerate human NP cells in conditioned medium (Bach et al., 2015). In addition, Hu et al. demonstrated that the stem cell niche could be isolated from the IVD and provided a method for the isolation and identification of NPMSCs (Hu et al., 2018). In the context of stem cell transplantation treatment, immune rejection, malignant stem cell proliferation, uncontrolled differentiation, and other factors should also be considered (Bagno et al., 2018). Therefore, the use of NP-derived stem cells in the present study was based on these considerations.

BMPs are involved in a variety of developmental processes, including bone, cartilage, and IVD formation (Carreira et al., 2015; Than et al., 2012). Currently available publications demonstrate that BMP-2 upregulates the gene expression and protein synthesis of ECM components in rabbits and human NP cells cultured *in vitro* (Lee et al., 2012); this phenomenon has been confirmed in rabbits *in vivo*, in which the use of adenovirus carrying BMP-2 treatment effectively delayed the process of circumferential disc degeneration (Leckie et al., 2012). Intradiscal BMP-2 injection has been shown to effectively stimulate ECM synthesis, restore disc height, and prevent degeneration (Li et al., 2017). However, a study by Huang et al. showed that certain negative effects, such as fibroblast proliferation, osteophyte formation, and cartilage endplate hypertrophy, were observed after 12 weeks of treatment with 100 µg of BMP-2 injected into the IVD of rabbits (Huang et al., 2007). This finding suggests that the growth factor dose, exposed cell type, and mode of growth factor application play important roles in guiding the cell phenotype during the construction of tissue-engineered NP. Kim et al. showed that exposure of human IVDs to BMP-2 using 3D beads did not induce an osteogenic response and successfully increased proteoglycan synthesis in NP cells (Kim et al., 2009). In addition, BMP-2 can form hydrogen bonds with fibrin-hyaluronic acid to achieve slow release (Li et al., 2017). These data show that BMP-2 is a beneficial growth factor that promotes the expression and synthesis of ECM.

Chitosan is widely used in various tissue engineering applications because of its excellent loading capacity (Yang et al., 2010; Shea and Mok, 2018). However, some studies have shown that chitosan has lower affinity for cells and growth factors; thus, chitosan needs to be combined with other materials or its surface needs to be modified to enhance its adhesion performance (Kwon et al., 2012). Thrombin can form soluble reticular fibrin molecules, and this structure is conducive to cell adhesion and proliferation. Its internal reticular structure is the basis of cell adhesion and sustained growth factor release (Chen et al., 2015). This issue has been a popular subject in tissue engineering studies aiming to solve the problem of malignant proliferation caused by growth factors with short half-lives, rapid consumption, and repeated action in the same location (Bozuyuk et al., 2018; Amidi et al., 2010). Some studies have shown that growth factors can form covalent bonds with composite chitosan microspheres; however, the slow-release properties are not ideal because of rapid release occurs in the early stage (Bozuyuk et al., 2018). In addition, Muzzarelli RA et al. demonstrated that growth factors can form crosslinks with fibrin gel via hydrogen bonds (Muzzarelli et al., 2015). This experiment used a double crosslinking structure to achieve the goal of sustained BMP-2 release. The results of the present study also demonstrated that this structure has ideal sustained release performance.

The BMP-2/Smad1/RUNX2 signaling pathway has typically been reported in previous studies to be involved in bone formation, and Smad1 protein interacts with RUNX2 to participate in osteoblastic gene expression and differentiation (Choi et al., 2001). Other studies have shown that Smad1 and RUNX2 coregulate the expression of collagen in osteoblasts (Pratap et al., 2011). In the present study, mechanical stress stimulated ITG A1 activation on the membrane surface of NPMSCs, which upregulated the expression of BMP-2, Smad1, and RUNX2, thus enhancing NPMSC proliferation, differentiation, and NP ECM expression. ITG A1 and BMP-2 were knocked down to investigate the correlation between ITG A1 and BMP-2 and the relationship between the upstream and downstream regions. The results confirmed the important role of the BMP-2/Smad1/RUNX2 signaling pathway in the expression profile and function of NPMSCs. However, the signal transduction pathway between ITG A1 and BMP-2 needs further study.

Injectable hydrogels are primarily used as emergency matrix substitutes for cartilage and disc regeneration (Stephanopoulos et al., 2013). These hydrogels have good hydrophilicity and are usually constructed by covalent or physical methods through three-dimensional crosslinking (Bao et al., 2020). Hydrogels mimic the stability and matrix composition of the natural disc ECM and are a potential choice for disc repair (Yang et al., 2017). Fibrin crosslinked using thrombin forms a network structure, which has strong viscous plasticity and is conducive to cell adhesion, growth, and proliferation (Riopel et al., 2015). Sharp et al. used fibrin scaffolds as carriers in spinal cord injury repair and achieved good effects (Sharp et al., 2012). Unlike synthetic and other natural materials, fibrin can effectively reduce inflammation (Ruangsawasdi et al., 2014). Therefore, inflammatory damage in the degenerated IVD is reduced, which is conducive to NP regeneration. We also carried out corresponding preliminary animal experiments and obtained some preliminary results. Subsequent animal experiments will become an important experimental focus of our research group.

Limitations of the study

The limitation of this study is that a comprehensive assessment of the mechanical properties and biocompatibility of the tissue-engineered NP was not performed, and our group will use three-dimensional finite element analysis to evaluate mechanical properties of the tissue-engineered spinal cord model. *In vivo* experiments to assess the biocompatibility of tissue-engineered NP will be conducted.

However, PMS and BMP-2 clearly play important roles in the construction of tissue-engineered NP, providing new information for the treatment of IVDD using injectable hydrogel scaffolds.

STAR★METHODS

Detailed methods are provided in the online version of this paper and include the following:

- KEY RESOURCES TABLE
- RESOURCE AVAILABILITY
  - Lead contact
  - Materials availability
  - Data and code availability
- EXPERIMENTAL MODEL AND SUBJECT DETAILS
  - Human subjects
  - Cell culture
- METHOD DETAILS
  - Identification of IVDSCs
  - Cell proliferation assay
  - Real-time quantitative polymerase chain reaction
  - Construction and evaluation of PMS system
  - Construction of chitosan composite fibrin gel scaffold
  - ELISA analysis
  - RNA interference
  - Immunofluorescence analysis
  - Western blot analysis
  - Histologic analysis
- QUANTIFICATION AND STATISTICAL ANALYSIS

SUPPLEMENTAL INFORMATION

Supplemental information can be found online at https://doi.org/10.1016/j.isci.2022.104405.

AUTHOR CONTRIBUTIONS

Conceptualization, Y.L. and L.N.; Formal analysis, Y.L., K.Y., and L.N.; Funding acquisition, G.G. and L.N.; Investigation, Y.L., G.G., K.Y., and L.N.; Methodology, Y.L., G.G., K.Y., and L.N.; Supervision, L.N.; Validation, Y.L., G.G., K.Y., and L.N.; Writing-original draft, Y.L., G.G., and L.N.; Writing-review and editing, Y.L., G.G., K.Y., and L.N.

DECLARATION OF INTERESTS

The authors declare no competing interests.

REFERENCES

Ahlgren, B.D., Lui, W., Herkowitz, H.N., Panjabi, M.M., and Guiboux, J.P. (2000). Effect of anular repair on the healing strength of the intervertebral disc: a sheep model. Spine (Phila Pa 1976) 25, 2165–2170.

Ahrens, M., Tsantrizos, A., Donkersloot, P., Martens, F., Lauweryns, P., Le Huec, J.C., Moszko, S., Fekete, Z., Sherman, J., Yuan, H.A., and Halm, H. (2009). Nucleus replacement with the DASCOR disc arthroplasty device: interim two-year efficacy and safety results from two prospective, non-randomized multicenter European studies. Spine (Phila Pa 1976) 34, 1376–1384.

Amidi, M., Mastrobattista, E., Jiskoot, W., and Hennink, W.E. (2010). Chitosan-based delivery systems for protein therapeutics and antigens. Adv. Drug Deliv. Rev. 62, 59–82.

Bach, F.C., De Vries, S.A., Krouwels, A., Creemers, L.B., Ito, K., Meij, B.P., and Tryfonidou, M.A. (2015). The species-specific regenerative effects of notochordal cell-conditioned medium on chondrocyte-like cells derived from degenerated human intervertebral discs. Eur. Cell Mater 30, 132–146. discussion 146-7.

Bagno, L., Hatzistergos, K.E., Balkan, W., and Hare, J.M. (2018). Mesenchymal stem cell-based therapy for cardiovascular disease: progress and challenges. Mol. Ther. : J. Am. Soc. Gene Ther. 26, 1610–1623.

Bao, W., Li, M., Yang, Y., Wan, Y., Wang, X., Bi, N., and Li, C. (2020). Advancements and frontiers in the high performance of natural hydrogels for cartilage tissue engineering. Front. Chem. 8, 53.

Bozuyuk, U., Dogan, N.O., and Kizilel, S. (2018). Deep insight into PEGylation of bioadhesive chitosan nanoparticles: sensitivity study for the Key parameters through artificial neural network model. ACS Appl. Mater. Interfaces 10, 33945–33955.

Brazil, D.P., Church, R.H., Surae, S., Godson, C., and Martin, F. (2015). BMP signalling: agony and antagony in the family. Trends. Cell. Biol. 25, 249–264.

Brown, S.J., Turner, S.A., Balain, B.S., Davidson, N.T., and Roberts, S. (2020). Is osteogenic differentiation of human nucleus pulposus cells a possibility for biological spinal fusion? Cartilage 11, 181–191.

Caplan, A.I. (2017). Mesenchymal stem cells: time to change the name. Stem. Cell. Transl. Med. 6, 1445–1451.

Carreira, A.C., Zambuzzi, W.F., Rossi, M.C., Astorino Filho, R., Sogayar, M.C., and Granjeiro, J.M. (2015). Bone morphogenetic proteins: promising molecules for bone healing, bioengineering, and regenerative medicine. Vitam. Horm. 99, 293–322.

Cazzanelli, P., and Wuertz-Kozak, K. (2020). MicroRNAs in intervertebral disc degeneration, apoptosis, inflammation, and mechanobiology. Int. J. Mol. Sci. 21, 3601.

Chen, Q., Zhang, Z., Liu, J., He, Q., Zhou, Y., Shao, G., Sun, X., Cao, X., Gong, A., and Jiang, P. (2015). A fibrin matrix promotes the differentiation of EMSCs isolated from nasal respiratory mucosa to myelinating phenotypical Schwann-like cells. Mol. Cells 38, 221–228.

Chen, X., Zhu, L., Wu, G., Liang, Z., Yang, L., and Du, Z. (2016). A comparison between nucleus pulposus-derived stem cell transplantation and nucleus pulposus cell transplantation for the treatment of intervertebral disc degeneration in a rabbit model. Int. J. Surg. 28, 77–82.

Cheng, H., Jiang, W., Phillips, F.M., Haydon, R.C., Peng, Y., Zhou, L., Luu, H.H., An, N., Breyer, B., Vanichakarn, P., et al. (2003). Osteogenic activity of the fourteen types of human bone morphogenetic proteins (BMPs). J. Bone. Joint. Surg. Am. 85, 1544–1552.

Chiang, C.J., Cheng, C.K., Sun, J.S., Liao, C.J., Wang, Y.H., and Tsuang, Y.H. (2011). The effect of a new anular repair after discectomy in intervertebral disc degeneration: an experimental study using a porcine spine model. Spine (Phila Pa 1976) 36, 761–769.

Choi, J.Y., Pratap, J., Javed, A., Zaidi, S.K., Xing, L., Balint, E., Dalamangas, S., Boyce, B., Van Wijnen, A.J., Lian, J.B., et al. (2001). Subnuclear targeting of Runx/Cbfa/AML factors is essential for tissue-specific differentiation during embryonic development. Proc. Natl. Acad. Sci. U S A 98, 8650–8655.

Clouet, J., Vinatier, C., Merceron, C., Pot-Vaucel, M., Hamel, O., Weiss, P., Grimandi, G., and Guicheux, J. (2009). The intervertebral disc: from pathophysiology to tissue engineering. Joint Bone Spine 76, 614–618.

Cunha, C., Almeida, C.R., Almeida, M.I., Silva, A.M., Molinos, M., Lamas, S., Pereira, C.L., Teixeira, G.Q., Monteiro, A.T., Santos, S.G., et al. (2017). Systemic delivery of bone marrow mesenchymal stem cells for in situ intervertebral disc regeneration. Stem Cells Transl. Med. 6, 1029–1039.

Dieleman, J.L., Baral, R., Birger, M., Bui, A.L., Bulchis, A., Chapin, A., Hamavid, H., Horst, C., Johnson, E.K., Joseph, J., et al. (2016). US spending on personal Health Care and public Health, 1996-2013. JAMA 316, 2627–2646.

Feng, G., Zhang, Z., Jin, X., Hu, J., Gupte, M.J., Holzwarth, J.M., and Ma, P.X. (2012). Regenerating nucleus pulposus of the intervertebral disc using biodegradable nanofibrous polymer scaffolds. Tissue. Eng. Part A 18, 2231–2238.

Gao, G., Shen, N., Jiang, X., Sun, H., Xu, N., Zhou, D., Nong, L., and Ren, K. (2016). Periodic mechanical stress activates EGFR-dependent Rac1 mitogenic signals in rat nucleus pulpous cells via ERK1/2. Biochem. Biophys. Res. Commun. 469, 723–730.

Govender, S., Csimma, C., Genant, H.K., Valentin-Opran, A., Amit, Y., Arbel, R., Aro, H., Atar, D., Bishay, M., Börner, M.G., et al. (2002). Recombinant human bone morphogenetic protein-2 for treatment of open tibial fractures: a prospective, controlled, randomized study of four hundred and fifty patients. J. Bone. Jt. Surg. 84, 2123–2134.

Hadjipavlou, A.G., Tzermiadianos, M.N., Bogduk, N., and Zindrick, M.R. (2008). The pathophysiology of disc degeneration: a critical review. J. Bone. Jt. Surg Br 90, 1261–1270.

Hegewald, A.A., Medved, F., Feng, D., Tsagogiorgas, C., Beierfuss, A., Schindler, G.A., Trunk, M., Kaps, C., Mern, D.S., and Thome, C. (2015). Enhancing tissue repair in annulus fibrosus defects of the intervertebral disc: analysis of a bio-integrative annulus implant in an in-vivo ovine model. J. Tissue. Eng. Regen. Med. 9, 405–414.

Hoogendoorn, R.J., Lu, Z.F., Kroeze, R.J., Bank, R.A., Wuisman, P.I., and Helder, M.N. (2008). Adipose stem cells for intervertebral disc regeneration: current status and concepts for the future. J. Cell. Mol. Med. 12, 2205–2216.

Hu, B., He, R., Ma, K., Wang, Z., Cui, M., Hu, H., Rai, S., Wang, B., and Shao, Z. (2018). Intervertebral disc-derived stem/progenitor cells as a promising cell source for intervertebral disc regeneration. Stem Cell Int. 2018, 7412304.

Huang, K.Y., Yan, J.J., Hsieh, C.C., Chang, M.S., and Lin, R.M. (2007). The in vivo biological effects of intradiscal recombinant human bone morphogenetic protein-2 on the injured intervertebral disc: an animal experiment. Spine (Phila Pa 1976) 32, 1174–1180.

Kadow, T., Sowa, G., Vo, N., and Kang, J.D. (2015). Molecular basis of intervertebral disc degeneration and herniations: what are the important translational questions? Clin. Orthop. Relat. Res. 473, 1903–1912.

Katz, J.N. (2006). Lumbar disc disorders and low-back pain: socioeconomic factors and consequences. J. Bone. Jt. Surg. Am. 88, 21–24.

Kim, H., Lee, J.U., Moon, S.H., Kim, H.C., Kwon, U.H., Seol, N.H., Kim, H.J., Park, J.O., Chun, H.J., Kwon, I.K., and Lee, H.M. (2009). Zonal responsiveness of the human intervertebral disc to bone morphogenetic protein-2. Spine (Phila Pa 1976) 34, 1834–1838.

Kwon, J.S., Kim, G.H., Kim, D.Y., Yoon, S.M., Seo, H.W., Kim, J.H., Min, B.H., and Kim, M.S. (2012). Chitosan-based hydrogels to induce neuronal

differentiation of rat muscle-derived stem cells. Int. J. Biol. Macromol. *51*, 974–979.

Le Maitre, C.L., Pockert, A., Buttle, D.J., Freemont, A.J., and Hoyland, J.A. (2007). Matrix synthesis and degradation in human intervertebral disc degeneration. Biochem. Soc. Trans. *35*, 652–655.

Leckie, S.K., Bechara, B.P., Hartman, R.A., Sowa, G.A., Woods, B.I., Coelho, J.P., Witt, W.T., Dong, Q.D., Bowman, B.W., Bell, K.M., et al. (2012). Injection of AAV2-BMP2 and AAV2-TIMP1 into the nucleus pulposus slows the course of inter-vertebral disc degeneration in an in vivo rabbit model. Spine J. : official J. North Am. Spine. Soc. *12*, 7–20.

Ledet, E.H., Jeshuran, W., Glennon, J.C., Shaffrey, C., De Deyne, P., Belden, C., Kallakury, B., and Carl, A.L. (2009). Small intestinal submucosa for anular defect closure: long-term response in an in vivo sheep model. Spine (Phila Pa 1976) *34*, 1457–1463.

Lee, K.I., Moon, S.H., Kim, H., Kwon, U.H., Kim, H.J., Park, S.N., Suh, H., Lee, H.M., Kim, H.S., Chun, H.J., et al. (2012). Tissue engineering of the intervertebral disc with cultured nucleus pulposus cells using atelocollagen scaffold and growth factors. Spine (Phila Pa 1976) *37*, 452–458.

Leung, V.Y., Chan, D., and Cheung, K.M. (2006). Regeneration of intervertebral disc by mesenchymal stem cells: potentials, limitations, and future direction. Eur. Spine J. *15* (*Suppl 3*), S406–S413.

Li, Z., Lang, G., Karfeld-Sulzer, L.S., Mader, K.T., Richards, R.G., Weber, F.E., Sammon, C., Sacks, H., Yayon, A., Alini, M., and Grad, S. (2017). Heterodimeric BMP-2/7 for nucleus pulposus regeneration-In vitro and ex vivo studies. J. Orthop. Res. *35*, 51–60.

Lo, K.W., Ulery, B.D., Ashe, K.M., and Laurencin, C.T. (2012). Studies of bone morphogenetic protein-based surgical repair. Adv. Drug Deliv. Rev. *64*, 1277–1291.

Murdoch, A.D., Grady, L.M., Ablett, M.P., Katopodi, T., Meadows, R.S., and Hardingham, T.E. (2007). Chondrogenic differentiation of human bone marrow stem cells in transwell cultures: generation of scaffold-free cartilage. Stem. Cells. *25*, 2786–2796.

Muzzarelli, R.A., El Mehtedi, M., Bottegoni, C., Aquili, A., and Gigante, A. (2015). Genipin-crosslinked chitosan gels and scaffolds for tissue engineering and regeneration of cartilage and bone. Mar. Drugs. *13*, 7314–7338.

Mwale, F., Ciobanu, I., Giannitsios, D., Roughley, P., Steffen, T., and Antoniou, J. (2011). Effect of oxygen levels on proteoglycan synthesis by intervertebral disc cells. Spine (Phila Pa 1976) *36*, E131–E138.

Neidlinger-Wilke, C., Mietsch, A., Rinkler, C., Wilke, H.-J., Ignatius, A., and Urban, J. (2012). Interactions of environmental conditions and mechanical loads have influence on matrix turnover by nucleus pulposus cells. J. Orthopaedic. Res. *30*, 112–121.

Oehme, D., Ghosh, P., Shimmon, S., Wu, J., Mcdonald, C., Troupis, J.M., Goldschlager, T., Rosenfeld, J.V., and Jenkin, G. (2014). Mesenchymal progenitor cells combined with pentosan polysulfate mediating disc regeneration at the time of microdiscectomy: a preliminary study in an ovine model. J. Neurosurg. Spine. *20*, 657–669.

Parker, S.L., Grahovac, G., Vukas, D., Vilendecic, M., Ledic, D., Mcgirt, M.J., and Carragee, E.J. (2016). Effect of an annular closure device (barricaid) on same-level recurrent disk herniation and disk height loss after primary lumbar discectomy: two-year results of a multicenter prospective cohort study. Clin. Spine. Surg. *29*, 454–460.

Poynton, A.R., and Lane, J.M. (2002). Safety profile for the clinical use of bone morphogenetic proteins in the spine. Spine *27*, S40–S48.

Pratap, J., Lian, J.B., and Stein, G.S. (2011). Metastatic bone disease: role of transcription factors and future targets. Bone *48*, 30–36.

Riopel, M., Trinder, M., and Wang, R. (2015). Fibrin, a scaffold material for islet transplantation and pancreatic endocrine tissue engineering. Tissue. Eng. Part B Rev. *21*, 34–44.

Risbud, M.V., and Shapiro, I.M. (2011). Notochordal cells in the adult intervertebral disc: new perspective on an old question. Crit. Rev. Eukaryot. Gene Expr. *21*, 29–41.

Ruangsawasdi, N., Zehnder, M., and Weber, F.E. (2014). Fibrin gel improves tissue ingrowth and cell differentiation in human immature premolars implanted in rats. J. Endod. *40*, 246–250.

Sakai, D., Mochida, J., Iwashina, T., Watanabe, T., Nakai, T., Ando, K., and Hotta, T. (2005). Differentiation of mesenchymal stem cells transplanted to a rabbit degenerative disc model: potential and limitations for stem cell therapy in disc regeneration. Spine (Phila Pa 1976) *30*, 2379–2387.

Sekine, C., Matsunaga, N., Okubo, Y., Hangai, M., and Kaneoka, K. (2021). Lumbar intervertebral disc degeneration does not affect muscle synergy for rowing activities. Appl. Bionics. Biomech. *2021*, 6651671.

Sharp, K.G., Dickson, A.R., Marchenko, S.A., Yee, K.M., Emery, P.N., Laidmae, I., Uibo, R., Sawyer, E.S., Steward, O., and Flanagan, L.A. (2012). Salmon fibrin treatment of spinal cord injury promotes functional recovery and density of serotonergic innervation. Exp. Neurol. *235*, 345–356.

Shea, G.K., and Mok, F. (2018). Optimization of Nanofiber scaffold properties towards nerve guidance channel design. Neural. Regen. Res. *13*, 1179–1180.

Stephanopoulos, N., Ortony, J.H., and Stupp, S.I. (2013). Self-assembly for the synthesis of functional biomaterials. Acta. Materialia. *61*, 912–930.

Su, W.Y., Chen, Y.C., and Lin, F.H. (2010). Injectable oxidized hyaluronic acid/adipic acid dihydrazide hydrogel for nucleus pulposus regeneration. Acta Biomater. *6*, 3044–3055.

Than, K.D., Rahman, S.U., Vanaman, M.J., Wang, A.C., Lin, C.-Y., Zhang, H., La Marca, F., and Park, P. (2012). Bone morphogenetic proteins and degenerative disk disease. Neurosurgery *70*, 996–1002.

Worthley, D.L., Churchill, M., Compton, J.T., Tailor, Y., Rao, M., Si, Y., Levin, D., Schwartz, M.G., Uygur, A., Hayakawa, Y., et al. (2015). Gremlin 1 identifies a skeletal stem cell with bone, cartilage, and reticular stromal potential. Cell *160*, 269–284.

Wu, M., Chen, G., and Li, Y.-P. (2016). TGF-β and BMP signaling in osteoblast, skeletal development, and bone formation, homeostasis and disease. Bone. Res. *4*, 16009.

Wuertz, K., Urban, J.P., Klasen, J., Ignatius, A., Wilke, H.J., Claes, L., and Neidlinger-Wilke, C. (2007). Influence of extracellular osmolarity and mechanical stimulation on gene expression of intervertebral disc cells. J. Orthop. Res. *25*, 1513–1522.

Yang, J., Zhang, Y.S., Yue, K., and Khademhosseini, A. (2017). Cell-laden hydrogels for osteochondral and cartilage tissue engineering. Acta. Biomater. *57*, 1–25.

Yang, Z., Duan, H., Mo, L., Qiao, H., and Li, X. (2010). The effect of the dosage of NT-3/chitosan carriers on the proliferation and differentiation of neural stem cells. Biomaterials *31*, 4846–4854.

Zhang, Y., Drapeau, S., Howard, S.A., Thonar, E.J., and Anderson, D.G. (2011). Transplantation of goat bone marrow stromal cells to the degenerating intervertebral disc in a goat disc injury model. Spine (Phila Pa 1976) *36*, 372–377.

Zhou, X., Wang, J., Fang, W., Tao, Y., Zhao, T., Xia, K., Liang, C., Hua, J., Li, F., and Chen, Q. (2018). Genipin cross-linked type II collagen/chondroitin sulfate composite hydrogel-like cell delivery system induces differentiation of adipose-derived stem cells and regenerates degenerated nucleus pulposus. Acta Biomater. *71*, 496–509.

STAR★METHODS

KEY RESOURCES TABLE

REAGENT or RESOURCE	SOURCE	IDENTIFIER
Antibodies		
APC anti-human CD34 Antibody	BioLegend	Cat#343510; RRID:AB_1877153
PE anti-human CD45 Antibody	BioLegend	Cat#368510; RRID:AB_2566370
FITC anti-human CD73 (Ecto-5′-nucleotidase) Antibody	BioLegend	Cat#344016; RRID:AB_2561809
FITC anti-human CD90 (Thy1) Antibody	BioLegend	Cat#328108; RRID:AB_893429
PE anti-human CD105 Antibody	BioLegend	Cat#323206; RRID:AB_755958
APC anti-human HLA-DR Antibody	BioLegend	Cat#307610; RRID:AB_314688
FITC Human IgG1 Isotype Control Recombinant Antibody	BioLegend	Cat#403508; RRID:AB_2847831
APC Human IgG1 Isotype Control Recombinant Antibody	BioLegend	Cat#403506
PE Human IgG1 Isotype Control Recombinant Antibody	BioLegend	Cat#403504
Anti-Integrin alpha 1 antibody	Abcam	Cat#ab200570
Recombinant Anti-BMP2 antibody [EPR20807]	Abcam	Cat#ab214821; RRID:AB_2814695
Anti-Smad1 antibody[EPR5522]	Abcam	Cat#ab126761; RRID:AB_11143606
Anti-RUNX2 antibody	Abcam	Cat#ab23981; RRID:AB_777785
Anti-Collagen II antibody	Abcam	Cat#ab34712; RRID:AB_731688
Anti-Aggrecan antibody[6-B-4]	Abcam	Cat#ab3778; RRID:AB_304071
Anti-GAPDH antibody[6C5] - Loading Control	Abcam	Cat#ab8245; RRID:AB_2107448
Goat Anti-Rabbit IgG H&L (HRP) antibody	Abcam	Cat#ab205718; RRID:AB_2819160
Goat Anti-Mouse IgG H&L (HRP) antibody	Abcam	Cat#ab205719; RRID:AB_2755049
Chemicals, peptides, and recombinant proteins		
Chitosan	Sigma-Aldrich	Cat#1105508
Sodium tripolyphosphate	Sigma-Aldrich	Cat#238503
Genipin	Sigma-Aldrich	Cat#G4796
TWEEN ® 80	Aladdin	Cat#T118633
Span™ 80	aladdin	Cat#S110840
Petroleum ether	aladdin	Cat#P119716
Paraffin liquid	aladdin	Cat#P104805
Human BMP-2 Recombinant Protein	Gibco	Cat#PHC7141
DAPI solution	Thermo Scientific	Cat#62248
Fibrinogen from human plasma	Sigma-Aldrich	Cat#F3879
Thrombin from human plasma	Sigma-Aldrich	Cat#T7009
BMP-2 siRNA (h)	Santa Cruz	Cat#sc-39738
Integrin α1/ITGA1/CD49a siRNA (h)	Santa Cruz	Cat#sc-43125
Critical commercial assays		
TRIzol Reagent	Invitrogen	Cat#15596018
RevertAid First Strand cDNA Synthesis Kit	Thermo Scientific	Cat#K1622
SYBR™ Green PCR Master Mix	Applied Biosystems	Cat#4309155
BMP-2 Human ELISA Kit	Invitrogen	Cat#EHBMP2
Cell Counting Kit-8	Dojindo Molecular Technologies	Cat#CK04
SuperSignal™ West Femto Maximum Sensitivity Substrate	Thermo Scientific	Cat#34095
Pierce BCA Protein Assay Kit	Thermo Scientific	Cat#23225

Continued

REAGENT or RESOURCE	SOURCE	IDENTIFIER
RIPA Lysis and Extraction Buffer	Thermo Scientific	Cat#89901
PMSF Protease Inhibitor	Thermo Scientific	Cat#36978
Experimental models: Cell lines		
Primary cultures of nucleus pulposus mesenchymal stem cells(NPMSCs)	This study	N/A
ex vivo nucleus pulposus explants cultures	This study	N/A
Oligonucleotides		
ACAN forward GATCCTTACCGTAAAGCCCATC	This study	N/A
ACAN reverse CTCCAGTCTCATTCTCAACCTC	This study	N/A
COL 2A1 forward CAAGAACAGCATTGCCTATCTG	This study	N/A
COL 2A1 reverse GATAACAGTCTTGCCCCACTTA	This study	N/A
Human GAPDH Endogenous Reference Genes Primers, 10 μM	Sangon Biotech	Cat#B661104-0001
Software and Algorithms		
FlowJo_v10.6.2	FlowJo	https://www.flowjo.com/
Prism 9	GraphPad	https://www.graphpad-prism.cn
ImageJ_v1.8.0	ImageJ	https://imagej.nih.gov/
Other		
DMEM-12 (Dulbecco's Modified Eagle Medium/Nutrient Mixture F-12)	Gibco	Cat#11320033
Fetal Bovine Serum	Gibco	Cat#12664025
Goat Serum, New Zealand Source	Gibco	Cat#16210064
Mesenchymal Stem Cell Chondrogenic Differentiation Medium	ScienCell	Cat#7551
Penicillin-Streptomycin solution	Gibco	Cat#15140122
0.25% Trypsin-EDTA	Gibco	Cat#25200072
Type II Collagenase	Gibco	Cat#17101015

RESOURCE AVAILABILITY

Lead contact

Further information and requests for resources and reagents should be directed to and will be fulfilled by the lead contact, Lu-ming Nong (L1uyyang031995@gmail.com).

Materials availability

This study did not generate new unique reagents.

Data and code availability

Data reported in this paper will be shared by the lead contact upon request. This paper does not report original code. Any additional information required to reanalyze the data reported in this paper is available from the lead contact upon request.

EXPERIMENTAL MODEL AND SUBJECT DETAILS

Human subjects

Degenerative NP tissue was collected from patients who underwent NP extraction in the spinal surgery department of the Changzhou Second People's Hospital. 6 female and 6 male patients (45.00 ± 14.26 years old) with lumbar disc herniation underwent percutaneous endoscopic lumbar discectomy in the operating room. Transported to the laboratory at 4 °C, and processed within 4h.

This study was reviewed by the Ethics Committee of Changzhou Second People's Hospital Affiliated to Nanjing Medical University, and informed consent was signed after full communication with patients and their families. This study followed the principles guidelines of the Declaration of Helsinki.

Cell culture

The degenerated NP of patients with IVD disease was removed under aseptic conditions by minimally invasive surgery. The NP tissue was placed into a culture dish containing PBS, mixed, and rinsed 3 times with PBS. The NP samples were cut into 1 mm^3 pieces, digested with 0.25% trypsin for 15 min, and neutralized with fetal bovine serum. After 24 hours of digestion with 0.2% type II collagenase, all impurities and liquids were discarded, and DMEM/F-12 containing 10% fetal bovine serum and 3.7 g/L calcium bicarbonate was added. The cells were incubated at 37 °C in 5% CO_2. The medium was replaced every 2-3 days, and the cells were passaged upon reaching 70-80% confluence. Second-generation cells were seeded in a 25 mm*25 mm culture flask at a density of $1*10^5$/mL. Experiments were performed when the cells reached 70-80% confluence.

METHOD DETAILS

Identification of IVDSCs

The identity of the NPMSCs was confirmed according to the criteria established by the International Society for Cellular Therapy (ISCT) (for example, plastic-adherent growth; CD105, CD73, and CD90 expression; and no CD45, CD34, or HLA-DR surface molecule expression). A flow cytometry assay was used to identify the phenotype of the cells.

Take the first passage of cells, digest 1 mL of 0.25% T-EDTA at 37°C for 5 minutes, add complete medium to terminate the digestion, and transfer the cells to a 15 mL conical centrifuge tube at 1500 rpm, centrifuge for 3 minutes, remove the supernatant, add 2% PBSF (PBS containing 2% FBS) to resuspend, count the cells, adjust the cell concentration to approximately 5-10×105 cells per 100 μL PBSF, and divide them into 10 groups. Group 1 was a blank control, 5 μL of IgG1 Isotype (APC-, PE-, FITC-) was added to groups 2-4 as an isotype control, and 5 μL of anti-CD34, CD45, CD73, CD90, CD105 and HLA-DR antibody were added to the other six groups. Incubated on ice for 15 minutes in the dark, and each group of reaction systems was supplemented with 2% PBSF to 500 μL, filtered and operated on the flow cytometer.

Cell proliferation assay

Cell proliferation was assessed every 2 days for each group after pre-differentiation by Cell Counting Kit-8 (CCK-8, Dojindo Molecular Technologies, Kumamoto, Japan) assay. The medium in each group was aspirated before testing, and the cells were incubated with DMEM/F-12 containing 5% CCK-8 at 37°C in 5% CO_2 for 2 hours. The supernatant was transferred to a 96-well plate with 100 μL in each well, and the absorbance of the samples in each group was measured at a wavelength of 450 nm. All data were calculated based on 3 valid samples.

Real-time quantitative polymerase chain reaction

The cells were completely lysed with TRIzol reagent (Invitrogen, USA), and RNA was extracted. Total RNA was reverse transcribed into cDNA using a RevertAid First Strand cDNA Synthesis Kit (Thermo Fisher, USA) according to the manufacturer's instructions. SYBR Green PCR was used for real-time PCR with a StepOnePlus system (Applied Biosystems, USA), and each group included 3 independent samples to ensure the validity of the data. Four target genes were detected using GAPDH as an internal control. The primers were synthesized by Sangon Biotech (Shanghai, China), and quantitative real-time PCR data were analyzed by the $2^{-\Delta\Delta Ct}$ method.

Construction and evaluation of PMS system

A "stress field culture system" (Figure S1.) with adjustable pressure intensity and frequency was constructed by connecting a periodic gas pressure device to a closed cell culture device. The pressure range of the system was 0~300 kPa, and the frequency range was 0~1 Hz. Second-generation NPMSCs were divided into two groups; one group was cultured under normal conditions, and the other group was cultured under mechanical stress (0~200 kPa, 0.1 Hz) (Gao et al., 2016).

Construction of chitosan composite fibrin gel scaffold

Initially, 2 mL of Tween 80 and 4 mL of Span 80 were placed in a beaker, and liquid paraffin was added to bring the volume to 100 mL. The mixture was placed under magnetic stirring until mixed evenly; then, 5 mL of 2% chitosan (2 g chitosan, Sigma, USA, added to a sufficient volume of double-distilled water to bring the volume to 100 mL) was added. The mixture was stirred until translucent, and then 4 mL of 1% sodium tripolyphosphate (Sigma, USA) was added. The mixture was stirred until it became creamy white, and then 3 mL of 1% genipin (Sigma, USA) was added. The pH was adjusted to 5.0, and the stirring was continued for 5 h. The reaction was stopped when blue particles appeared at the bottom of the cup, and the solution was placed into a centrifuge tube; the rotation speed was adjusted to 1000 rpm/min, and the tube was centrifuged for 10 minutes. Next, the upper layer of liquid was removed, and the particles were rinsed 2 times with petroleum ether, anhydrous ethanol, and PBS. The obtained particles were freeze-dried to yield prepared microparticles. Chitosan microspheres were prepared by high-speed centrifugation and freeze-drying of 5 mg of the particles in PBS (5 mL) containing 1 μg of BMP-2 (Gibco, USA) for 3 h.

Fibrin solution with a mass concentration of 100 mg/mL was prepared by dissolving fibrin monomer powder in normal saline at 37°C to promote dissolution. Thrombin powder was dissolved in normal saline to prepare thrombin solution with a concentration of 20 U/mL. The composite fibrin scaffolds were prepared by mixing 50 μL of the thrombin solution with 5 mg of the composite chitosan microspheres and 50 mL of the fibrinogen solution in 24-well plates.

ELISA analysis

Then, 5 mg of chitosan microspheres, 100 μL of fibrin gel scaffolds, and 100 μL of chitosan composite fibrin gel scaffolds were placed in three 2 mL EP tubes, 1 mL of PBS (pH=7.4) *in vitro* sustained release solution was added to the EP tubes, and the tubes were placed at 37°C. In a shaker with a rotational speed of 1000 rpm/min in the incubator, the supernatant of each EP tube was taken at different time points (1, 6, and 12 h and 1, 2, 4, 6, 8, 10, 12, and 14 d), and 500 μL samples were added at the same time. The sample concentration was determined by an ELISA kit, each sample was assayed three times, and the average value was calculated. According to the results, a sustained release curve was drawn to compare the sustained release effects of the three samples.

RNA interference

BMP-2 and ITG A1 expression in NPMSCs was silenced with siRNAs (Santa Cruz, California) according to the standard protocol. High silencing efficiency was verified in the corresponding experiments.

Immunofluorescence analysis

NPMSCs were seeded on coverslips in 24-well plates, fixed with 4% paraformaldehyde, and infiltrated by PBS with 0.2% Triton X-100. The samples were cleaned, blocked with 3% goat serum in PBS at 37°C, and incubated with a primary antibody against BMP-2 (1:50, Abcam). The samples were then treated with a goat anti-rabbit antibody at 37°C for 2 h and stained with 0.1 g/mL DAPI (Thermo Scientific, USA) for 5 min. Images were acquired using a microscope (Olympus, New York).

Western blot analysis

The cells were washed with cold PBS 3 times; total protein was extracted with RIPA buffer containing 1% PMSF, and the protein concentration was measured with a quantitative BCA protein kit (Thermo Fisher, USA). The following primary antibodies were used:anti-COL 2A1 antibody (1:1000, Abcam); anti-ACAN antibody (1:1000, Abcam); anti-BMP-2 antibody (1:1000, Abcam); anti-ITG A1 antibody (1:1000, Abcam), anti-Smad1 antibody (1:1000, Abcam), anti-RUNX2 antibody (1:1000, Abcam), and anti-GAPDH antibody (1:1000, Abcam). GAPDH was used for normalization of the data. The membrane was incubated with the corresponding horseradish peroxidase (HRP)-labeled secondary immunoglobulin G conjugate (1:2000, Abcam) at room temperature for 1 h. Protein bands were visualized and detected using an enhanced chemiluminescence (Thermo Fisher, USA) system. The experiments were performed in triplicate.

Histologic analysis

After we successfully constructed tissue-engineered NP, each group was treated for 6 weeks before histological analysis. Tissue-engineered NP specimens were fixed in formaldehyde and embedded in paraffin

after dehydration. Sections of each specimen were stained with H&E and evaluated according to a histological grading system. All tests were performed in at least three areas of each sample.

QUANTIFICATION AND STATISTICAL ANALYSIS

Statistical significance was assessed by ANOVA, and the Mann–Whitney U test was used as the post hoc test. The data are expressed as the mean $\pm$ standard deviation (SD). Unless indicated otherwise, significance was set at * $p < 0.05$, ** $p < 0.01$, and *** $p < 0.001$.